Desalination and Water Treatment 320 (2024) 100691

Contents lists available at ScienceDirect

Desalination and Water Treatment

journal homepage: www.sciencedirect.com/journal/desalination-and-water-treatment/

Prosopis juliflora biochar for adsorption of sulfamethoxazole and ciprofloxacin from pharmaceutical wastewater

Hailu Ashebir[a], Jemal Fito Nure[b,*], Abebe Worku[a], Titus A.M. Msagati[c]

[a] Addis Ababa Science and Technology University Department of Environmental Engineering, Collage of Engineering, Addis Ababa, Ethiopia
[b] Department of Chemical and Metallurgical Engineering, University of the Witwatersrand, 1 Jorissen St, Ag, 2000, South Africa
[c] Institute for Nanotechnology and Water Sustainability (iNanoWS), College of Science, Engineering, and Technology, University of South Africa, Florida Science Campus, Johannesburg 1710, South Africa

ARTICLE INFO

Keywords:
Adsorbent
Antibiotic residue
Environmental pollution
Kinetics
Removal
Wastewater

ABSTRACT

This study aimed to synthesize **the** biochar of Prosopis juliflora (PJ) and apply it to the adsorption of antibiotic residues sulfamethoxazole (SMZ) and ciprofloxacin (CIX) from pharmaceutical industry wastewater. The PJ biochar was synthesized using the pyrolysis method and characterized by proximate analysis, TGA, SEM-EDX, FTIR, XRD, and BET methods. The moisture content, volatile matter, ash content, and fixed carbon were found to be 6.4 %, 72.3 %, 3.0 %, and 18.3 %, respectively. Moreover, biochar characteristics were described by a high BET surface area of 875 m^2/g, various FTIR peaks with different functional groups, high TGA thermal stability at increasing temperature, amorphous XRD structure, and high SEM surface morphology, and major EDX carbon compositions of 97 %. These analysis results demonstrated insights into the potential and nature of biochar adsorbent. The maximum adsorption of SMZ and CIX was found to be 98.7 % and 97.8 %, respectively, at a contact time of 120 min, initial concentration of 50 mg/L, pH (5 for CIX and 8 for SMZ), and adsorbent dose of 1 g/L for a synthetic solution. On the other hand, COD and TOC of real wastewater were reduced from 2498 to 514 mg/L and 1050 to 124 mg/L during the real wastewater treatment. Target pollutants concentration in real wastewater was found to be 8.29 and 5.3 mg/L for CIX and SMZ and their removal efficiency was obtained as 80.4 % and 76.7 % respectively. The obtained experimental data were best fitted with the Langmuir isothermal model at $R^2 = 0.999$, implying the adsorbent surface is homogeneous and monolayer. Similarly, the adsorption kinetics process was well described by a pseudo-second-order kinetics model for both SMZ and CIX at $R^2 = 0.999$. Finally, the non-linear intra-particle diffusion graphs suggest that chemical adsorption is the main influencing factor for overall kinetics. In conclusion, using PJ biochar is a promising precursor in advancing adsorbents for removing contaminants from industrial wastewater to address environmental pollution challenges.

1. Introduction

In the occurrences of environmental pollution, the emergence of contaminants in pharmaceutical wastewater has raised concerns within the scientific community and prompted extensive investigations into primary sources of water pollution [1,2]. Among pharmaceutical pollutants, sulfamethoxazole (SMZ) and ciprofloxacin (CIX) are the two widely used synthetic fluoroquinolone antibiotics with significant implications for public health and the environment [3,4]. The annual consumption of CIX in 2015 was estimated to rise to 2318 tons which underscores their global impact [5–7]. Overuse of antibiotics including SMZ extends beyond human medicine to agriculture, where antimicrobial drugs are increasingly utilized. Practically, the growth and promotion are leading to a significant entry of antimicrobials into various environmental components such as hospital effluents, drug manufacturing plants, sewage, and agricultural runoff [7–9]. Consequently, up to 90 % of consumed antibiotic doses are excreted through urine into water sources or human feces, resulting in detectable concentrations of CIX and SMZ in water bodies, and pharmaceutical effluents [10,11]. SMZ and CIX are commonly found in water and pharmaceutical effluents which can pose risks to human health and contribute to antibiotic resistance and potentially increasing mortality rates [12–19]. The escalating risk of antibiotic resistance stresses, the urgent need for comprehensive measures to address this critical health

* Corresponding author.
E-mail address: fitojemal120@gmail.com (J.F. Nure).

https://doi.org/10.1016/j.dwt.2024.100691
Received 31 March 2024; Received in revised form 29 June 2024; Accepted 2 August 2024

issue and its long-term consequences on global public health and well-being [13,14]. However, conventional wastewater treatment faces challenges in removing antibiotics efficiently due to longer reaction times, high energy use, and the requirement of expensive equipment [15–17]. However, various techniques like advanced oxidation processes [18], biodegradation [19], photolytic/photocatalytic treatment [20], chemical reduction [21], and adsorption [22–24], have been explored for antibiotic removal, as a cost-effective solution. Among these, adsorption stands out as a cost-effective and highly efficient technology for the removal of persistent antibiotics [25,26]. Carbonaceous materials like graphene oxide and activated carbon have shown potential for adsorption due to their high surface area, better stability, and feasibility of mass production [27–29]. Particularly, biochar adsorption of organic micropollutants from industrial wastewater has been reported which is pressing the need to explore new carbon-based adsorbents with rapid adsorption rates, specific surface reactivity, and high adsorption capacity [30].

A carbon-rich biochar material derived from waste biomass and offers promise as an efficient adsorbent for hydrophobic pollutants due to its aromaticity, high surface area, and multi-surface functionalities [31–33]. The choice of raw material and production methods significantly influence the adsorption efficiency of biochar, and surface properties [34–36]. Specifically, biochar derived from agricultural waste typically shows high porosity and surface area. The adsorbent efficiency can vary depending on the specific composition of the raw material and processing conditions. In contrast, biochar derived from woody biomass sources offers better stability and enhances the adsorption of various contaminants with good retention [37,38]. On the other hand, the production of biochar from woody biomass may need more energy-intensive processes which is potentially increasing its environmental footprint with its high surface area. Additionally, factors such as pH, adsorbent dose, and the chemical nature of pollutants can significantly influence the effectiveness of biochar in adsorbing pollutants. This condition can necessitate tailored approaches to optimize its performance [39]. In line with sustainable development goals, Prosopis juliflora (PJ) weed-derived biochar presents potential adsorbents in searching for a sustainable solution for removing pharmaceutical residues using adsorption technology. This is due to its high surface area and aromaticity which enhances its adsorption efficiency. By using isotherm models and conducting kinetic analyses, this study aimed to uncover the adsorption mechanisms and dynamics of SMZ and CIX. Generally, previous biochar studies have recognized the potential of biochar in wastewater purification role, but they lack a comprehensive understanding of its adsorption behavior, in real wastewater. Therefore, this research aimed to bridge that gap by investigating optimal adsorption conditions, suitable isotherm models, and kinetics for efficient removal of pharmaceutical residues from real wastewater. The key findings and implications of this study were to explore the potential of PJ biochar as an adsorbent and enhance its adsorption capacity for the remediation of pharmaceutical residues. The findings of this study might contribute to the development of sustainable schemes for addressing antibiotic contamination in water sources and maximizing the usage of biochar as an effective adsorbent. Hence, this study highlights the urgent need for proactive measures to tackle antibiotic contamination in water sources and emphasizes the promising role of biochar in mitigating this pressing environmental issue.

2. Methods and materials

2.1. Chemicals

In this study, biomass derived from the invasive weed PJ was sourced from the Afar regional state of Ethiopia and utilized as primary raw material for biochar production as an adsorbent. The chemicals employed, including SMZ ($C_{10}H_{11}N_3O_3S$), and CIX ($C_{17}H_{18}FN_3O_3$), were obtained from Ethiopian Pharmaceutical Manufacturing S.C. NaOH with > 98 % and HCl > 37 % purity were obtained from Sisco Research Laboratories Pvt. Ltd, India. All solutions were precisely prepared with distilled water, and working solutions of SMZ and CIX were prepared by dissolving 100 mg in 1 L of each pharmaceutical product in distilled water and afterward diluting to the needed concentration. Throughout the research, all chemicals and reagents used maintained a laboratory-grade standard and underwent no additional purification processes.

2.2. Synthesize of biochar

Synthesis of PJ biochar was accomplished using the pyrolysis method as depicted in Fig. 1. The plant material was cut into pieces of ~5 cm in length and 2 cm in diameter and exposed to sunlight for three weeks. Subsequently, it was dried in an oven for 24 h at 105℃ [34]. Then, oven-dried PJ was crushed by hammer mill mortar and standardized using a 60-mesh sieve size to achieve uniformly calcinated biochar during calcination. The uniformly crushed PJ was then subjected to different temperatures (500, 550, and 600 ℃) with a 10 ℃/min heating rate for 2 h in a muffle furnace under the flow of nitrogen gas (99 % purity) to create an inert environment. Then, the synthesized biochar was washed using distilled water to eliminate soluble salts and other water-soluble impurities to enhance its adsorption capacity for the intended target pollutants [35]. Then, the washed biochar was dried again in an oven at 80 ℃ for 24 h and packed in an airtight plastic bag for characterization and application of the adsorption experiments and further analysis.

2.3. Biochar characterization

To investigate deeper into the characteristics of biochar, a thorough proximate analysis becomes essential. This analysis covers moisture content (MC), volatile matter (VM), ash content (AC), and fixed carbon (FC). By following standardized methodologies outlined by ASTM, a comprehensive analysis of biochar offers valuable insights into potential uses. Analysis of all proximate was conducted by adapting the standard method of ASTAM and D1762–84 [36]. Surface characteristics and structural properties of the PJ biochar underwent compressive examination using various techniques. The surface morphology analysis and quantitative chemical composition analysis, scanning electron microscopy (SEM) coupled with an Energy Dispersive X-ray (EDX) analyzer were employed, operating at 30 kV (Hitachi, Japan). Before imaging, samples were mounted on carbon tape and gold-suspended. The functional groups were investigated by using FTIR (Perkin Elmer, Annapolis, MD, USA), recording the spectrum in transmission mode over wavelengths ranging from 4000 to 400 cm^{-1} [40]. X-ray Diffraction (XRD) analysis, utilizing Powdered-XRD on a Smart Lab SE X-ray apparatus from Rigaku, Japan, was used to study variations in the crystal structure of the biochar. Thermogravimetric Analysis (TGA) was performed on a Shimadzu TGA-50 H instrument from Japan, with a heating rate of 10 °C per min, up to 1000 °C, in a nitrogen atmosphere. This analysis was conducted to evaluate the thermal stability and degradation behavior of the biochar over a range of temperatures. It provided insights into temperature-dependent changes in weight and helped understand the decomposition patterns of the biochar under different conditions. The surface area of the biochar was studied by the Horriba SA9603 USA instrument. This method involves nitrogen gas adsorption at liquid nitrogen temperature to measure the amount of gas adsorbed onto the surface of the biochar. The data obtained from this adsorption isotherm was used to calculate the specific surface area, providing valuable information about the porosity and surface characteristics of the biochar. The determination of the point zero charge (pH_pzc) for the biochar was conducted using the salt addition method. To achieve this, six 250 mL Erlenmeyer flasks were prepared, each containing 50 mL of 0.1 M NaCl solution. The initial pH of these solutions was adjusted within the range of 2 to 11 using 0.1 M HCl and

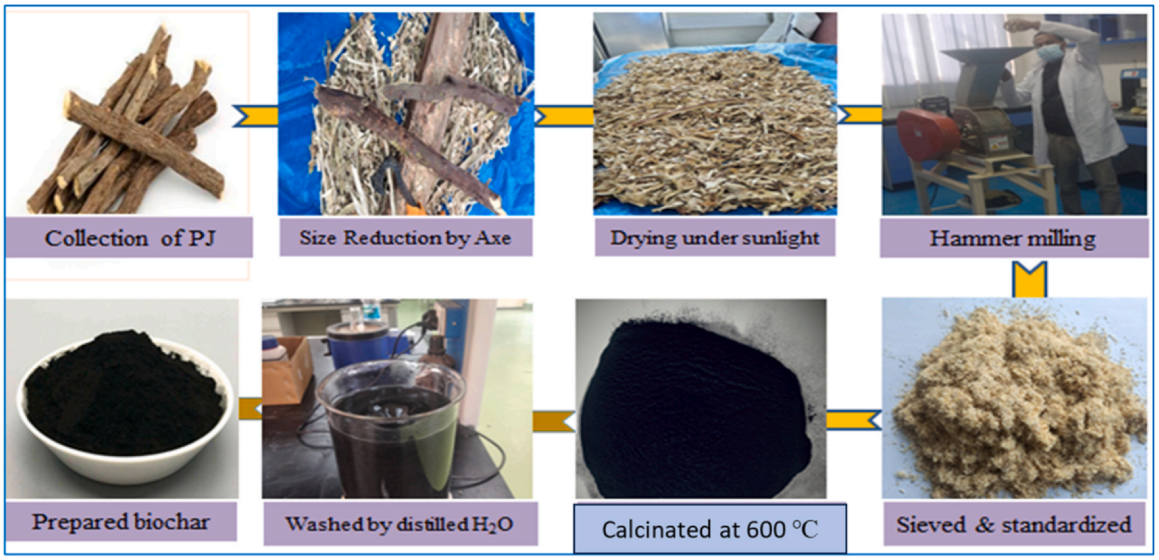

Fig. 1. Diagrammatic description of PJ biochar preparation stages.

Table 1
Proximate analysis of raw PJ and synthesized biochar of PJ.

Parameters	Present report (%)		Reported from Literature (%)
	PJ biochar	Raw PJ	PJ Biochar
Moisture content	6.42	7.24	5.6[52]
Volatile Matter	72.26	81.12	86.67[53]
Ash content	2.99	2.23	3.6[54]
Fixed Carbon	18.25	9.28	4.23[53]

0.1 M NaOH solutions. Subsequently, 0.5 g of biochar was added to each solution, and the mixtures were stirred at room temperature (~25 °C) using an orbital shaker at 150 rpm for 24 h. Following this, the final pH of the solutions was recorded, and the change in pH (ΔpH = pH_f - pH_i) was calculated. Finally, a graph illustrating the change in pH versus initial pH was plotted to identify the pH_pzc, represented by the x-intercept on the graph [40].

2.4. Experimental methods

The efficiency of biochar adsorption is directly impacted by various process parameters. These include pH range for CIX and SMZ set between 3 and 11, initial concentrations of CIX and SMZ varying between 5 and 65 mg/L, and amount of adsorbent varying between 0.5 to 3 g/L, contact time spanning from 15 to 120 min, and agitation on an orbital shaker was adjusted to moderate range of 250 rpm that allows for efficient mixing and equilibration without causing excessive mechanical stress on the biochar [41]. Throughout the study, samples were systematically withdrawn at specified intervals, subjected to filtration using Whatman 0.42 µm, and subsequently centrifuged at 5000 rpm for 10 min. The concentrations of SMZ and CIX in the samples were quantified using a UV-Vis spectrometer (UV-3600 Series, Shimadzu Co. Ltd., Japan). The wavelengths of 265 and 278 nm obtained from scanning within a quartz cuvette were used for SMZ and CIX analysis, respectively [42,43]. The evaluation of biochar adsorption performance in pollutant removal involved determining the pollutant percentage removal (%*R*) using Eq. 1 and adsorption efficiency (q_t) (Eq. 2).

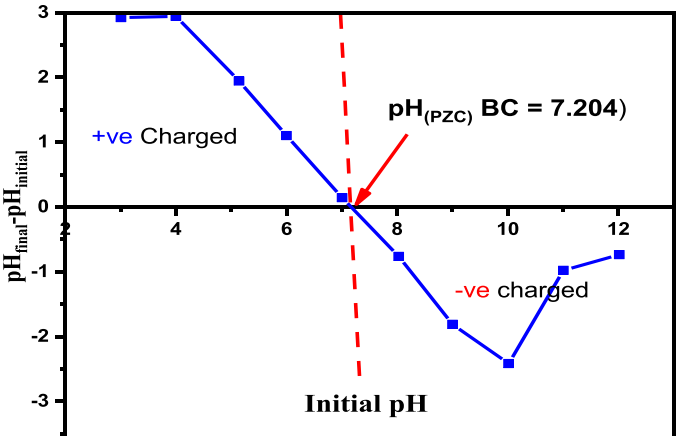

Fig. 2. Point zero charge of PJ biochar calcinated at 600 °C.

$$R\ \% = \frac{C_i - C_t}{C_i} * 100 \quad (1)$$

where C_i (mg/L) indicates the initial concentration of CIX and SMZ pollutants and C_t (mg/L) represents the highest concentration recorded after adsorption treatment.

$$q_e = \frac{(C_i - C_t)}{m} * V \quad (2)$$

q_e represents the adsorption ability of biochar, V denotes the volume of the solution and m denotes the mass of the biochar used. These equations are crucial for quantifying the effectiveness of biochar in removing pollutants and providing valuable insights into the percentage removal and adsorption capacity. The adsorption data were analyzed by isotherm and kinetic models, and the most suitable model was selected using linear regression. This process involved determining the factors and determination coefficients (R^2) for the adsorption isotherm models.

2.5. Adsorption isotherms

The Langmuir isotherm model is well-suitable for describing homogeneous and monolayer adsorption processes occurring on a surface with a limited number of identical sites. It assumes a uniform surface with equal sorption energy at each binding site while neglecting interaction between adsorbed molecules. This model determines the maximum adsorption capacity for complete monolayer coverage and is expressed linearly by Eq. 3.

$$\frac{1}{q_e} = \frac{1}{Q_o} + \frac{1}{Q_o C_e K_L} \quad (3)$$

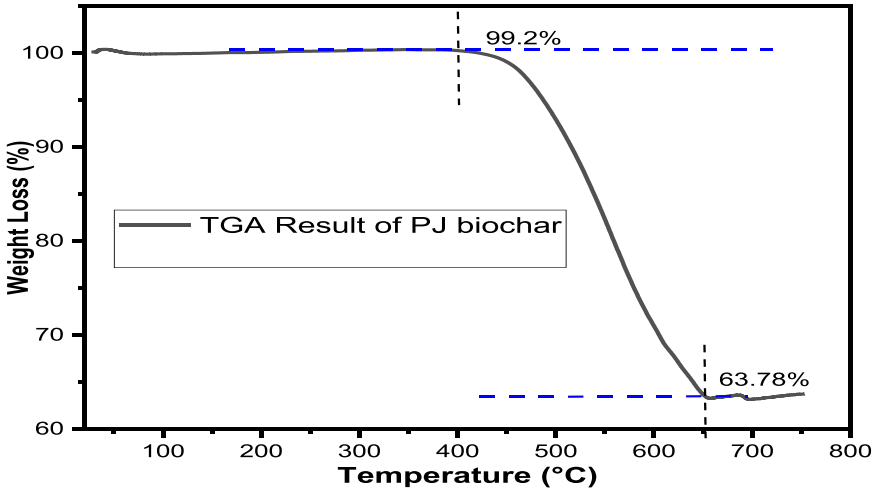

Fig. 3. TGA analysis for PJ biochar calcinated at 600 °C.

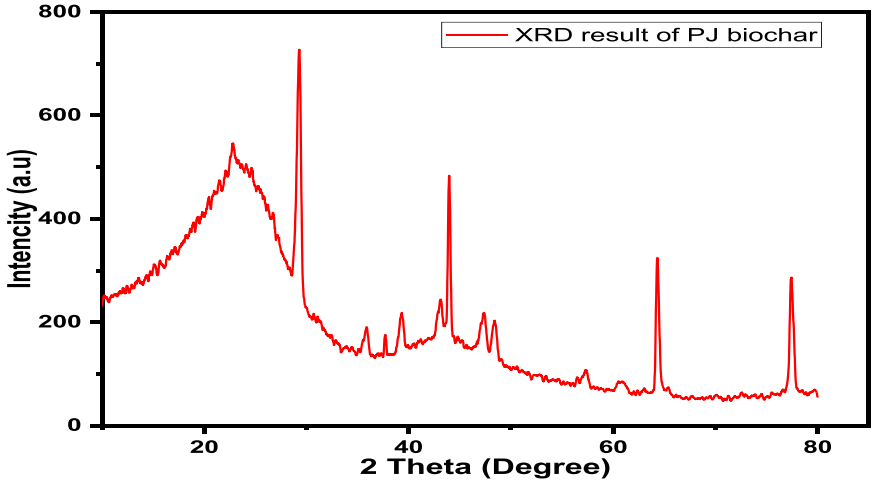

Fig. 4. XRD result of PJ biochar calcinated at 600 °C.

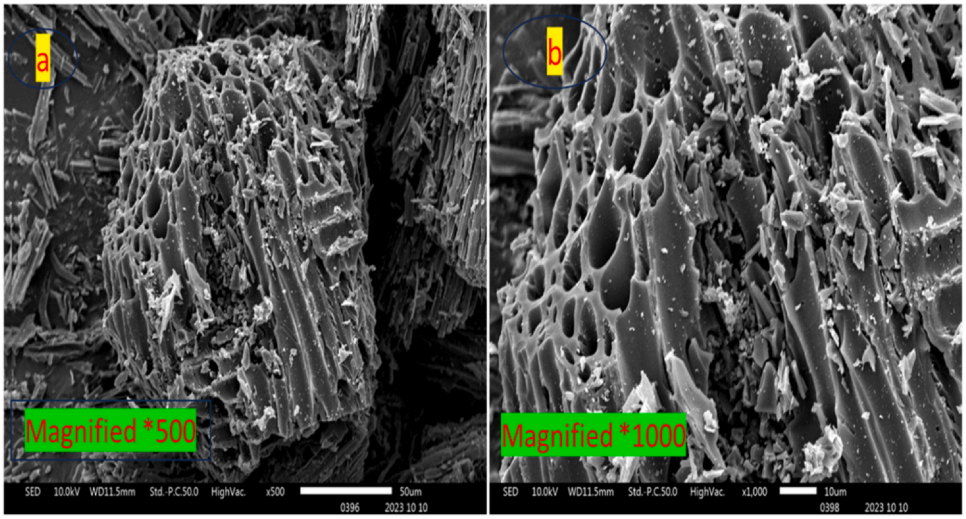

Fig. 5. SEM results were magnified at different resolutions a), 500 μm and b) 1000 μm.

In this context, q_e (mg/g) denotes the adsorption capacity of SMZ and CIX at equilibrium. K_L (L/mg) represents the Langmuir adsorption constant, while Q_0 (mg/g) indicates the maximum adsorption quantity determined by the model. Ce (mg/L) stands for the equilibrium concentration after adsorption. The Freundlich isotherm model, illustrates a heterogeneous surface with an exponential dispersal of active centers, suggesting infinite surface coverage, and implying multilayer adsorption. The concise expression for the Freundlich isotherm is often represented by Eq. 4.

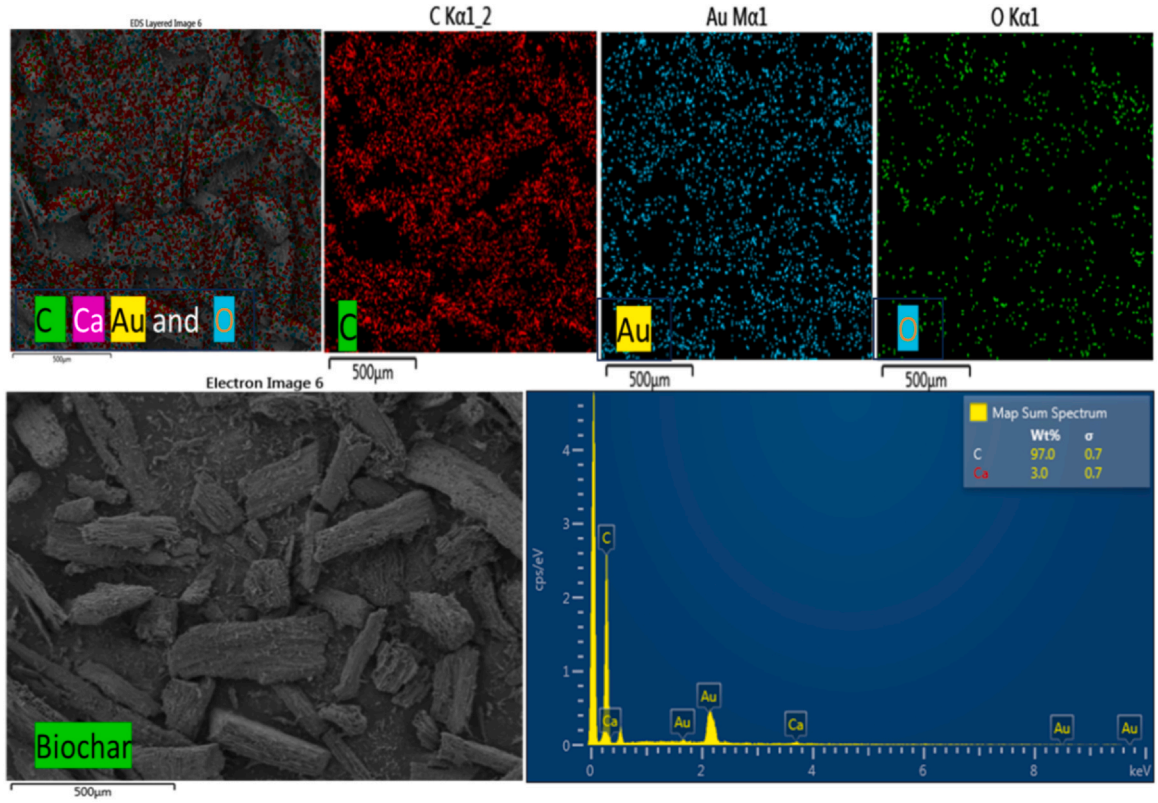

Fig. 6. Mapping result of SEM-EDX including the elemental composition of PJ biochar.

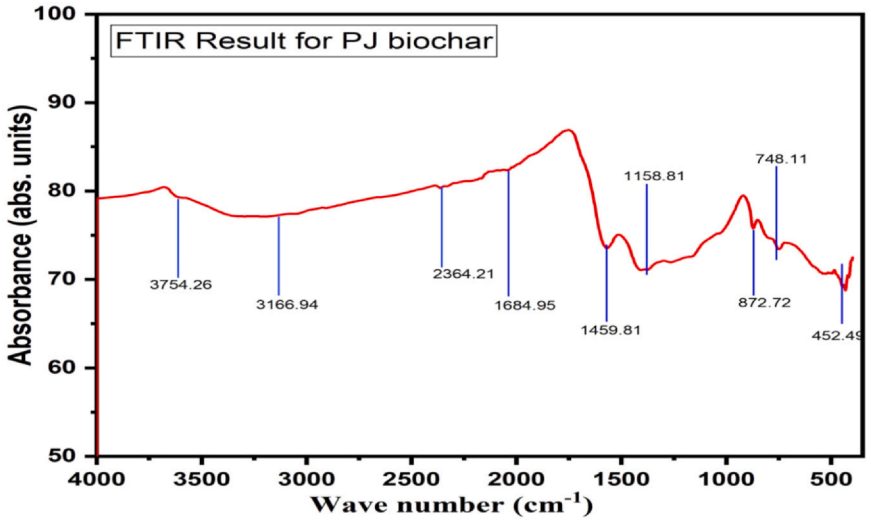

Fig. 7. FTIR result of PJ biochar calcinated at 600 °C.

$$logq_e = \frac{1}{n}\log C_e + \log K_F \quad (4)$$

where $logq_e$ signifies the logarithm of the adsorption capability, 1/n denotes the adsorption strength, $logC_e$ represents the logarithm of the equilibrium concentration and $logK_F$ stands for the Freundlich constants associated with adsorption capacity. Dubinin introduced a versatile isotherm analysis technique, which is considered more general than the Langmuir type [44]. In this model, the Dubinin-Radushkevich monolayer capacity in this model is written as follows in Eq. 5 and the model concept is described using Eqs. 6–8 including the linear Temkin isotherm model.

$$\ln Q = \ln Q_m - k\varepsilon^2 \quad (5)$$

$$q_e = \frac{RT}{B_T}\ln(a_T C_e) \quad (6)$$

$$q_e = B\ln a_T + B\ln Ce \quad (7)$$

$$B = \frac{RT}{b_T} \quad (8)$$

The Q_m values (mg/g) signify the monolayer capacity according to the Dubinin-Radushkevich model. The Polanyi potential is expressed as $\varepsilon = RT\ln(1 + 1/Ce)$, where R is the universal gas constant (8.314 J/mol K), and β is a sorption energy-related parameter [45]. In this context, it represents the equilibrium constant of the bond relative to its highest energy.

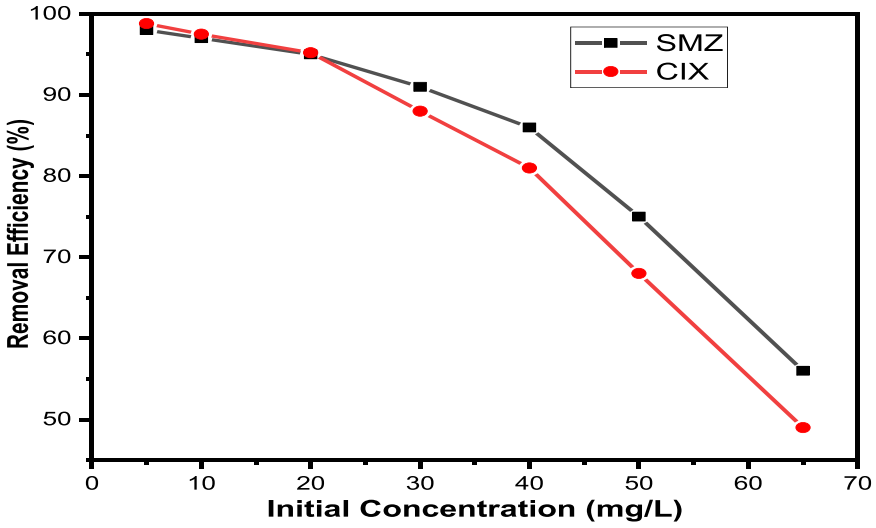

Fig. 8. Impact of Initial concentration on the adsorptive removal of CIX and SMZ at pH = (5 for CIX and 8 for SMZ), 120 min contact time, and 1 g/L adsorbent dose.

2.6. Adsorption kinetics

The adsorption kinetics of the system was explained using pseudo-first-order and pseudo-second-order equations using Eqs. 9 and 10.

$$q_t = q_e[1 - \exp(-k_f t)] \quad) \tag{9}$$

$$\frac{dq_t}{d_t} = k_2(q_e - q_t)^2 \tag{10}$$

Eq. 10 expresses the quantity of SMZ and CIX adsorbed per unit mass of the biochar q_t at any given time (t) in mg/g. The equilibrium capacity q_e denotes the calculated amount, while the equilibrium rate constant k_2 is derived from the pseudo-second-order equation. By integrating Eq. 10 with boundary conditions from $q_t = 0$ to q_t at t = 0 to t, can simplify and linearize it to derive Eq. 11.

$$\frac{t}{q_e} = \frac{1}{k_2 q_e^2} + \frac{1}{q_e}(t) \tag{11}$$

The values of k_2 and q_e were determined by analyzing the intercept and the slope of the plot obtained from t/q_t versus t. In intra-particle diffusion (IPD), the frequently employed to ascertain the adsorbate species diffusion mechanism from the aqueous phase. The sorption uptake may be shown to vary almost proportionally with $t^{0.5}$ using the following Eq. 12.

$$q_t = K_{int} t^{0.5} + C \tag{12}$$

K_{int} = mg/g is intra-particle diffusion rate constant. The boundary layer's thickness was indicated by the symbol $t^{0.5}$.

2.7. Adsorption of real wastewater

The physicochemical properties and biochar application in treating actual wastewater were investigated following the determination of optimal parameters except for initial concentration. Wastewater samples were sourced from the "Cadila pharmaceutical" industry in Gelan City, located east of Addis Ababa, Ethiopia. Adsorption experiments were conducted using real wastewater to evaluate the adsorbent's performance under optimal conditions: pH of 5, contact time of 120 min, and adsorbent dose of 1 g/L. The effectiveness of the adsorbent was assessed via spectrophotometric analysis of absorbance, and results were reported in concentration (mg/L) along with removal efficiency and other relevant physicochemical parameters.

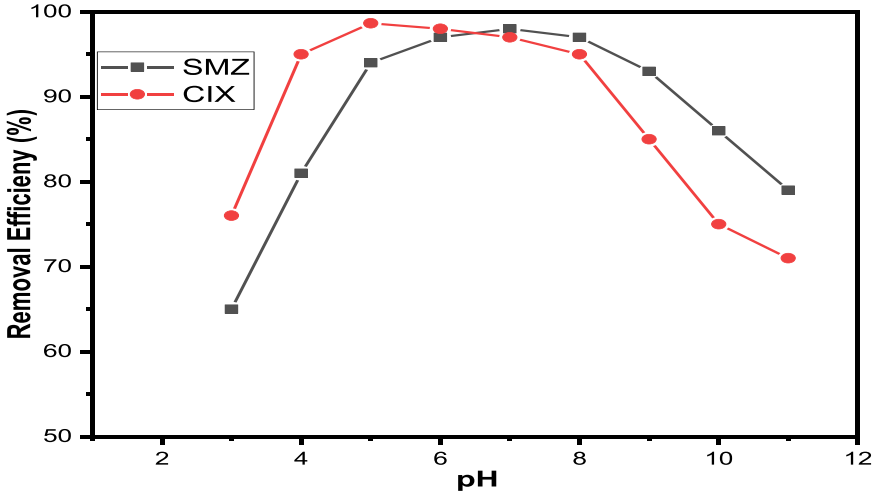

Fig. 9. Impact of Initial pH on the adsorptive removal of CIX and SMZ at 50 mg/L initial concentration, 120 min contact time, and 1 g/L adsorbent dose.

Table 2
Isotherm model parameters for adsorption of SMZ and CIX on PJ biochar calcinated at 600℃.

Isotherm models		Pharmaceutical residue pollutants	
		SMZ	CIX
Langmuir	q_{max} (mg/g)	49.776	91.432
	K_L (L/mg)	0.036	0.018
	Equation	Y = 0.5527x + 0.020	Y = 0.6115x + 0.011
	R^2	0.997	0.997
Freundlich	K_F (mg/g)/(mg/L)	2.11	2.166
	1/n	0.743	0.903
	Equation	Y = 0.7438x + 0.324	Y = 0.8066x + 0.335
	R^2	0.960	0.982
Dubinin–Radushkevich	q_{max} (mg/g)	19.07	20.201
	R^2	0.725	0.741
	K	9.71325E−07	1.12004E−06
	Equation	Y = −1E−06x + 2.9481	Y = −1E−06x + 3.006
	ε (/mol)	717.46	668.141
Temkin	K_T (L/mg)	0.718	0.632
	B_T (J/mol)	8.291	9.483
	R^2	0.882	0.894

Table 3
Comparing the different adsorbents' adsorption capabilities.

Type of Biomass	Adsorbent	Pollutant	Parameters	Qe (mg/g)	References
Rice straw	MoS2-coated biochar	CIX	Inc. conc = 20 mg/L, Contact time = 12 hrs, dose = 3.9 g/L	39.5	[80]
Pomelo peel	Chitosan biochar beads	CIX	Inc. conc = 50 mg/L, contact time = 120 min, dose = 1.25 g/L	36.76	[81]
Prosopis juliflora	Biochar	CIX	Inc. conc = 100 mg/L, contact time = 5 hrs, dose = 1.2 g/L	74.54	[5]
Prosopis juliflora	Biochar	CIX	Inc. conc = 50 mg/L, Contact time = 120 min, dose = 1 g/L	49.77	this study
Prosopis juliflora	Biochar	SMZ	Inc. conc = 50 mg/L, Contact time = 120 min, dose = 1 g/L	91.43	this study
Tea waste	Biochar	SMZ	Int. conc = 50 mg/L, dose = 1 g/L, Contact time = 72 hrs	33.81	[82]
Spent coffee grounds	Activated biochar	SMZ	Int. conc = 50 mg/L, dose = 1 g/L, Contact time = 72 hrs	88.10	[83]

Keys: inc. = initial and conc = concentration

3. Result and discussion

3.1. Biochar characteristics

3.1.1. Proximate analysis

The proximate analysis of raw Prosopis juliflora (RPJ) and synthesized biochar Prosopis juliflora (PJB) showcases the remarkable shifts in composition throughout pyrolysis. From the reduction in MC to the increase in FC levels, these changes align with typical biomass conversion patterns. The increase of AC in PJB indicates the concentration of inorganic minerals during pyrolysis, showcasing the importance of temperature and calcination time in biochar synthesis. As depicted in Table 1, the drop of MC from 9.2 to 4.8 % in PJB signifies effective water removal during high-temperature treatment, which was comparable findings with previous studies on biochar synthesis, emphasizing the role of temperature in proximate composition [46]. A decrease of VM from 81.3 to 72.9 % in PJB reveals the release of volatile organic chemicals during pyrolysis. Understanding the impact of VC reduction on biochar properties and applications [47]. The FC content increased from 16.3 in RPJ to 22.3 % in PJB, suggesting the presence of carbonaceous material due to the elimination of volatile components. The AC, ascending from 2.23 in RPJ to 2.99 % in PJB specifies the accumulation of inorganic minerals. Exploring the implications of AC variations in biochar for enhancement of water and environmental remediation [48,49]. This shift from RPJ to PJB aligns with normal pyrolysis patterns reported in biomass conversion, where volatile components are reduced, leading to an increase in FC and ash accumulation [50,51]. In conclusion, the proximate study of PJB

Table 4
Parameters of the kinetics model for the adsorption of CIX and SMZ on PJ biochar calcinated at 600 °C.

Kinetics model		SMZ	CIX
Pseudo-first order	K_1 (/min)	−0.000041	−5.58333E−05
	q_{cal} (mg/g)	1	0.998
	Equation	Y = 0.0049x - 0.0012	Y = −0.0067x - 0.0019
	R^2	0.927	0.818
	K_2 (g/mg/min)	0.208	0.208
Pseudo-second order	q_{cal} (mg/g)	16.605	16.608
	Equation	Y = 0.0602x + 0.0174	Y = 0.0604x + 0.0188
	R^2	0.999	0.999
	C	1.609	2.029
Intraparticle diffusion	K_{int} (mg/g.$min^{0.5}$)	0.288	0.080
	R^2	0.973	0.667

Table 5
Phyco-chemical characteristics of real pharmaceutical industry wastewater.

Parameters	Before Treatment	After Treatment	Literature (results before treatment)
pH	6.78	6.7	7.2[88]
TDS mg/L	1109	151	2155[96]
Conductivity (μS/cm)	2228	2567	7253[89]
Salinity	1.13	1.55	1.43[90]
Turbidity (NTU)	450	70	742[91]
TOC (mg/L)	1050	124	1295[93]
BOD (mg/L)	762	98	1097[54]
COD (mg/L)	2498	541	2268[54]
Nitrate (mg/L)	57	12.1	-
Phosphate (mg/L)	1.42	0.96	-
Sulphate (mg/L)	82	47	400. [95]
Sulfamethoxazole (mg/L)	5.3	1.04	0.5 −14 [97]
Ciprofloxacin (mg/L)	8.29	1.93	7.19[98]

indicates considerable variations in composition, indicating its potential uses in carbon sequestration, water treatment, and soil improvement.

3.1.2. Point of zero charge

The pH_pzc serves as a vital indicator defining the surface charge attributes of material such as biochar. As depicted in Fig. 2, it represents the pH value at which the material's surface achieves electrical neutrality, indicating equilibrium between positive and negative charges. Grasping the pH_pzc of biochar holds significance as it can impact various intermediate processes, including the adsorption and degradation of pollutants such as SMZ and CIX. Biochar often shows a pH_pzc in the moderately acidic to neutral range, often around 7.0 to 7.5. In this case, the reported pH_pzc for biochar is 7.2. This shows that at a pH below 7.2, the surface of biochar will contain a net positive charge, making it suitable for adsorbing negatively charged molecules. Conversely, with a pH over 7.2, the surface can contain a net negative charge, which attracts positively charged organisms [55].

3.1.3. BET analysis

Biochar synthesized was calcinated under varied temperatures of 500, 600, and 650 ℃ which resulted in variation of surface areas 752, 875.78, and 823 m^2/g. The surface area increase that is observed as the calcination temperature rises is consistent with the common behavior of carbonaceous materials. The initial phases of pyrolysis produced porous structures at 500 ℃ with a biochar surface area of 752 m^2/g. The material showed increased carbonization and extra formation of porous structures when the calcination temperature increased to 600℃. This led to a considerable increase in surface area to 875.8 m^2/g. But at 650℃ a trend reversal was observed, and the surface area slightly decreased to 823 m^2/g. According to published research, this decrease at higher temperatures could be caused by excessive carbonization-induced pore collapse or coarsening [56]. The ideal calcination temperature for enhancing surface area appears to be within the 600℃ range. This temperature range provides a balance between maintaining a highly porous structure and successful carbonization. The findings underline the necessity of carefully selecting pyrolysis or calcination temperatures to adapt biochar characteristics for specific applications, highlighting the need for a thorough comprehension behavior of the material under various thermal treatments.

Additionally, the mechanism of adsorption for both drugs based on the characterization of surface area, and functional groups of the biochar determines its adsorption capacity and affinity towards specific molecules. For instance, the high surface area of our biochar, as revealed by BET surface area analysis and pore size distribution studies, provides ample active sites for adsorption. Additionally, the presence of functional groups such as hydroxyl (-OH), carboxyl (-COOH), and phenolic (-Ph) groups, as identified through FTIR spectroscopy, enhances the adsorption of polar molecules like CIX and SMZ through electrostatic interactions, hydrogen bonding, and π-π stacking. Moreover, the SEM analysis highlights the porous morphology and heterogeneous surface of the biochar, facilitating the diffusion and accessibility of the target pollutants to the active sites. Overall, the comprehensive characterization of biochar provides valuable insights into its adsorption mechanism, paving the way for the design and optimization of efficient adsorbents for pharmaceutical wastewater treatment.

3.1.4. TGA analysis

The TGA graph depicted in Fig. 3 features a decline with a weight loss of only 0.8 % between 37 to 400℃ and a rapid decline with a weight loss of 35.42 % between 400 to 650℃, suggesting a complicated thermal behavior of the biochar. Such a pattern suggests multiple processes occurring during the heating or decomposition of the sample. The initial small reduction of weight may have resulted from the removal of moisture or other volatile components. This is a common incidence in TGA analyses, where low-temperature occurrence often

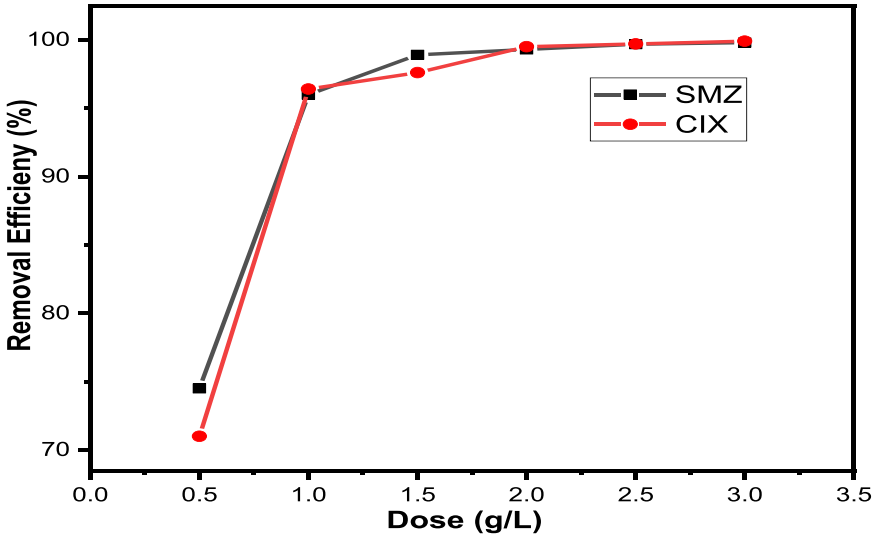

Fig. 10. Impact of adsorbent dose on the adsorptive removal of CIX and SMZ at pH = (5 for CIX and 8 for SMZ), 120 min contact time, and 50 mg/L initial concentration.

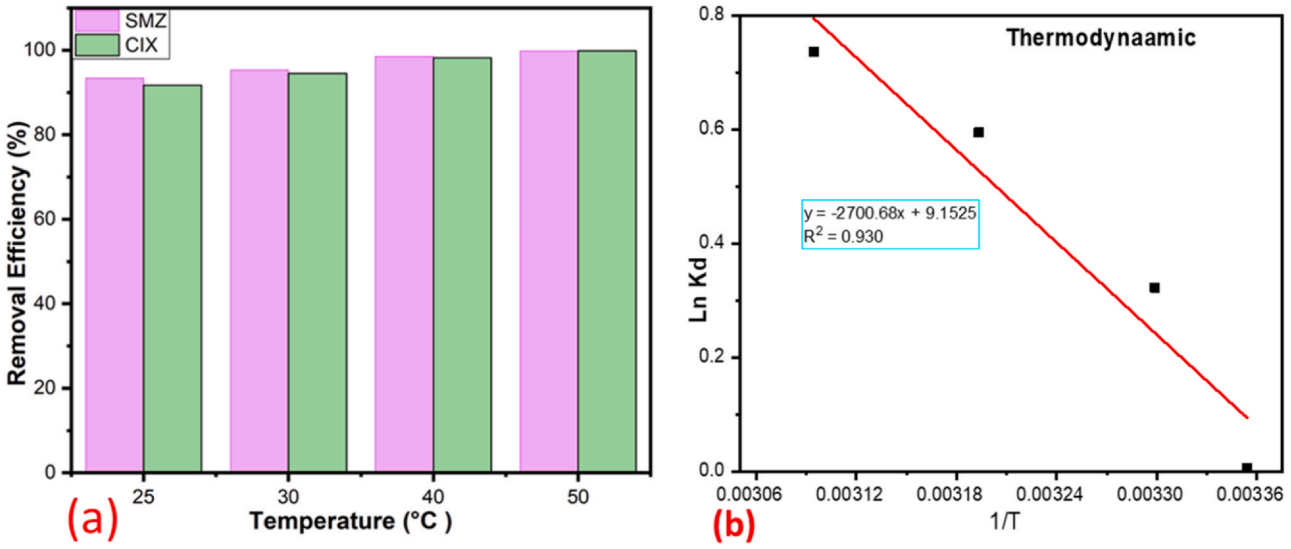

Fig. 11. (a) Impact of Temperature and (b) Thermodynamic Analysis on Adsorptive Removal of CIX and SMZ.

represents the evaporation or desorption of surface-bound or loosely bound molecules [34]. The high weight loss in the second stage, which was followed by a fast decrease, points to a more dramatic shift, in keeping with numerous studies [34]. The sharp drop indicates that the composition or structure of the material has changed quickly, most likely because of the start of a thermal degradation process. The disparity in weight loss between the first and second points indicates a shift in the dominant mechanism governing the behavior.

3.1.5. XRD analysis

The XRD peaks are presented in Fig. 4 and the observed value at 2 Theta = 29.1° indicates the exitance of certain crystalline phases and/or mineral components. Similarly, the peaks at 2 Theta = 44.0° peak might represent crystallite cellulose or other organic polymers present in the original biomass, 64.2° might be linked to minerals such as calcite ($CaCO_3$) or dolomite ($CaMg(CO_3)_2$), which can be found in plant tissues [57], and 77.5° might represent minerals like sulfate minerals that are frequently found in plant cellulose [58]. Depending on the makeup of the feedstock and the surrounding environment, these minerals may have been present in the initial biomass or may have been added during the pyrolysis process [59]. The crystalline nature of the biochar, as indicated by these XRD peaks, may affect its properties and applications. Crystallinity can affect biochar's reactivity, porosity, and stability, thereby impacting its performance in various environmental and agricultural applications. Moreover, the intensity and sharpness of these peaks can provide insights into the degree of crystallinity and structural order within the biochar. Further analysis, such as peak broadening or fitting to crystalline models, could elucidate the specific crystallographic phases present and their relative proportions. Overall, the XRD results show that the biochar is crystalline, providing important details for understanding its structure-property relationships and optimizing its application potential in fields such as carbon sequestration, soil remediation, and wastewater treatment [53].

3.1.6. SEM-EDX

The SEM study result provides an accurate perspective of the surface shape as shown in Fig. 5a and b. The outcomes demonstrate porous character by showing the presence of multiple pores. Upon magnification, the SEM images depict a homogenous complex surface porosity structure, emphasizing the unique surface architecture. The SEM analysis reveals that block particles are still present on the surface despite the existence of these pores, indicating possible problems in achieving absolute homogeneity. The structural configuration exposes a unique and complicated pattern that resembles a web of connected honeycombs [60]. This conclusion is consistent with past research that demonstrates how surface roughness impacts material properties [61]. Additionally, a significantly high BET surface area supports the SEM results even more. Notably, a remarkably high BET surface area measurement confirms the SEM results and demonstrates remarkable porosity [62]. Because of its honeycomb-like network structure and homogenous porosity, biochar has the potential adsorbent with morphological qualities that can be used in a range of sectors. On the other hand, improving the block particle dispersion might serve as a focal point for enhancing the material's overall uniformity and usefulness in specific applications [63,64].

Complementing the SEM analysis, SEM-EDX data offer fundamental insights into the composition of the biochar, completing the picture of the SEM investigation. As depicted in Fig. 6. the result reveals a predominant composition of carbon, constituting 97 % of the material. Additionally, calcium and oxygen are present at 3 %, indicating a minor inorganic matter. The high carbon content aligns with the observed porous structures and honeycomb-like network revealed in the SEM images. Carbonaceous materials often exhibit intricate morphologies, and the high carbon percentage underscores the porous and complex surface features. The presence of calcium and oxygen, although in a lower proportion, introduces an inorganic component to the material. This compositional finding suggests a composite material with both organic and inorganic elements, adding depth to our knowledge and structure of the biochar. A thorough SEM-EDX investigation is crucial for a comprehensive characterization of the material, as its composition may contribute to special qualities and possible uses [65–67]. Future investigations could focus on customizing the elemental makeup to improve material characteristics for intended uses, offering insightful knowledge for material engineering and development.

3.1.7. FTIR analysis

The adsorbent of FTIR was carried out and the results of different wavenumbers like 3854.28, 3751.90, 2864.36, 1684.95, 1559.61, 1158.81, 872.95, 748.11, 452.49, 435.01, 418.48, and 410.67 cm^{-1} with distinct peaks are displayed in Fig. 7. The distinct peak observed at 3854.28 cm^{-1} suggests the presence of hydroxyl groups, typically associated with alcohols or phenolic compounds [5]. Additionally, the peaks at 3751.90 and 2864.36 cm^{-1} indicate the stretching vibrations of hydroxyl groups in phenols and aliphatic alcohols, respectively [68,69]. Strong absorption at 1684.95 cm^{-1} is indicative of aldehydes or ketones that have undergone carbonyl stretching. Furthermore, the bands at 1559.61 and 1158.81 cm^{-1} are attributed to aromatic ring vibrations and C-O stretching in ethers, respectively. A variety of

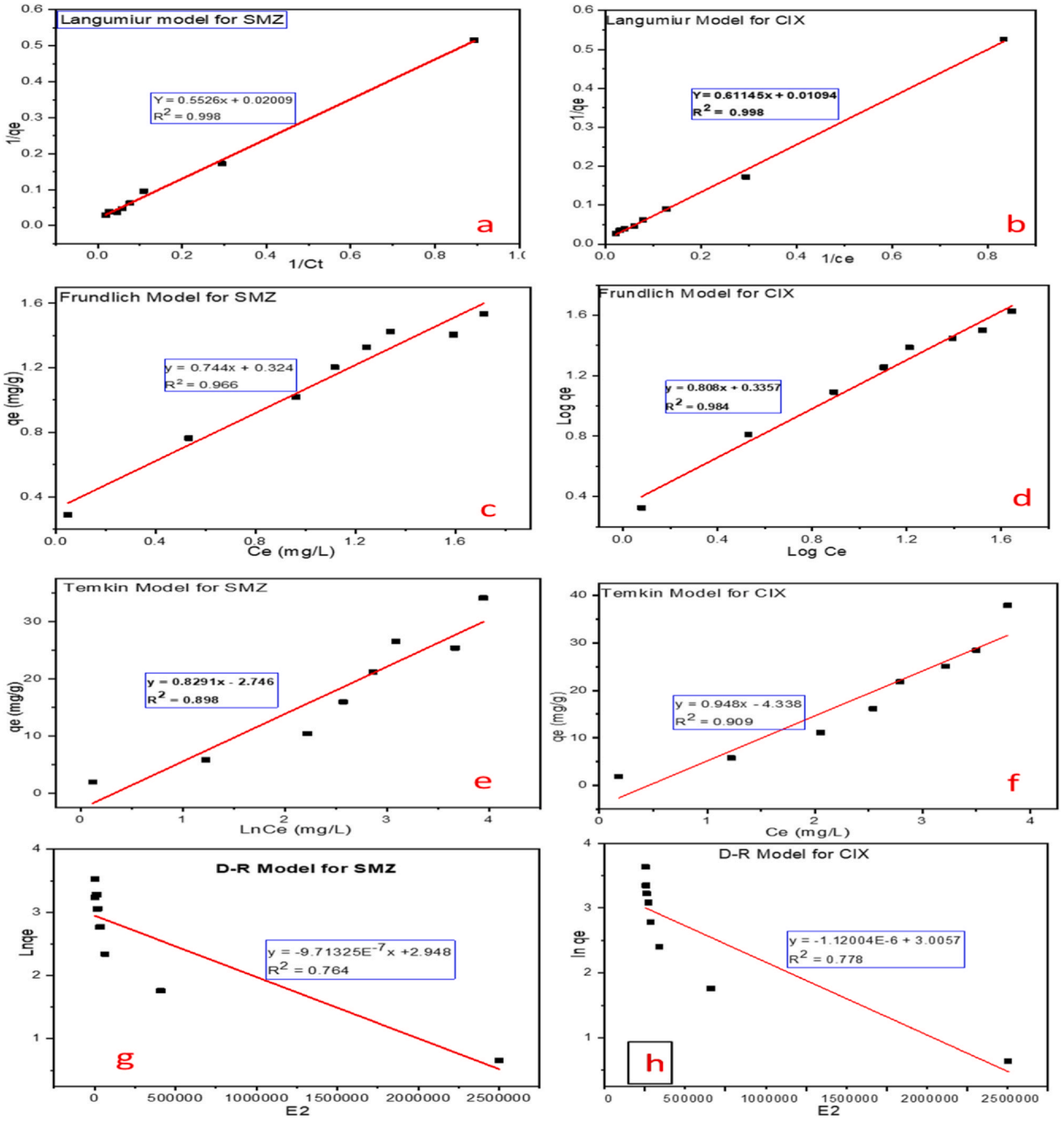

Fig. 12. Isotherm Models for CIX and SMZ Removal: (a) Langmuir for SMZ, (b) Langmuir for CIX, (c) Freundlich for CIX, (d) Freundlich for SMZ, (e) Temkin for CIX, (f) Temkin Model for SMZ, (g) D-R for CIX, and (h) D-R for SMZ.

functional groups are represented by the peaks seen at 872.95, 748.11, 452.49, 435.01, 418.48, and 410.67 cm^{-1}. These groups include C-H bending in alkanes, C-Cl stretching in alkyl chlorides, and C-N stretching in amines. These detected peaks align with the chemical fingerprint of plant biomass, indicating the existence of cellulose, hemicellulose, lignin, and other organic constituents. The FTIR results are consistent with studies on similar plant materials, providing a molecular perspective on the composition of biochar [70]. Since the characteristic peaks show the presence of organic molecules appropriate for biomass conversion, the identified functional groups support the potential uses of biochar in bioenergy [71]. The detailed FTIR analysis enhances our understanding of biochar chemical composition, opening the door for tailored utilization in various industrial and environmental applications.

3.2. Factors affecting the adsorption of SMZ and CIX

3.2.1. Initial concentration

The initial pollutant concentrations of SMZ and CIX impact the batch adsorption process as demonstrated in Fig. 8. To evaluate the adsorptive capacity of biochar and the adsorption isotherm, by adjusting the initial levels of SMZ and CIX between 5 and 65 mg/L while keeping other variables constant. Initially, the removal of SMZ and CIX was most effective at lower concentrations, but it increased as the concentrations became higher. This suggests that the active sites of the adsorbent became saturated as the concentrations rose. The adsorption capacity of biochar for SMZ increased from 11.2 mg/g at 5 mg/L to 54.56 mg/g at 65 mg/L, and for CIX, it increased from approximately 8.4 to 40.5 mg/g within the same concentration range, and these results

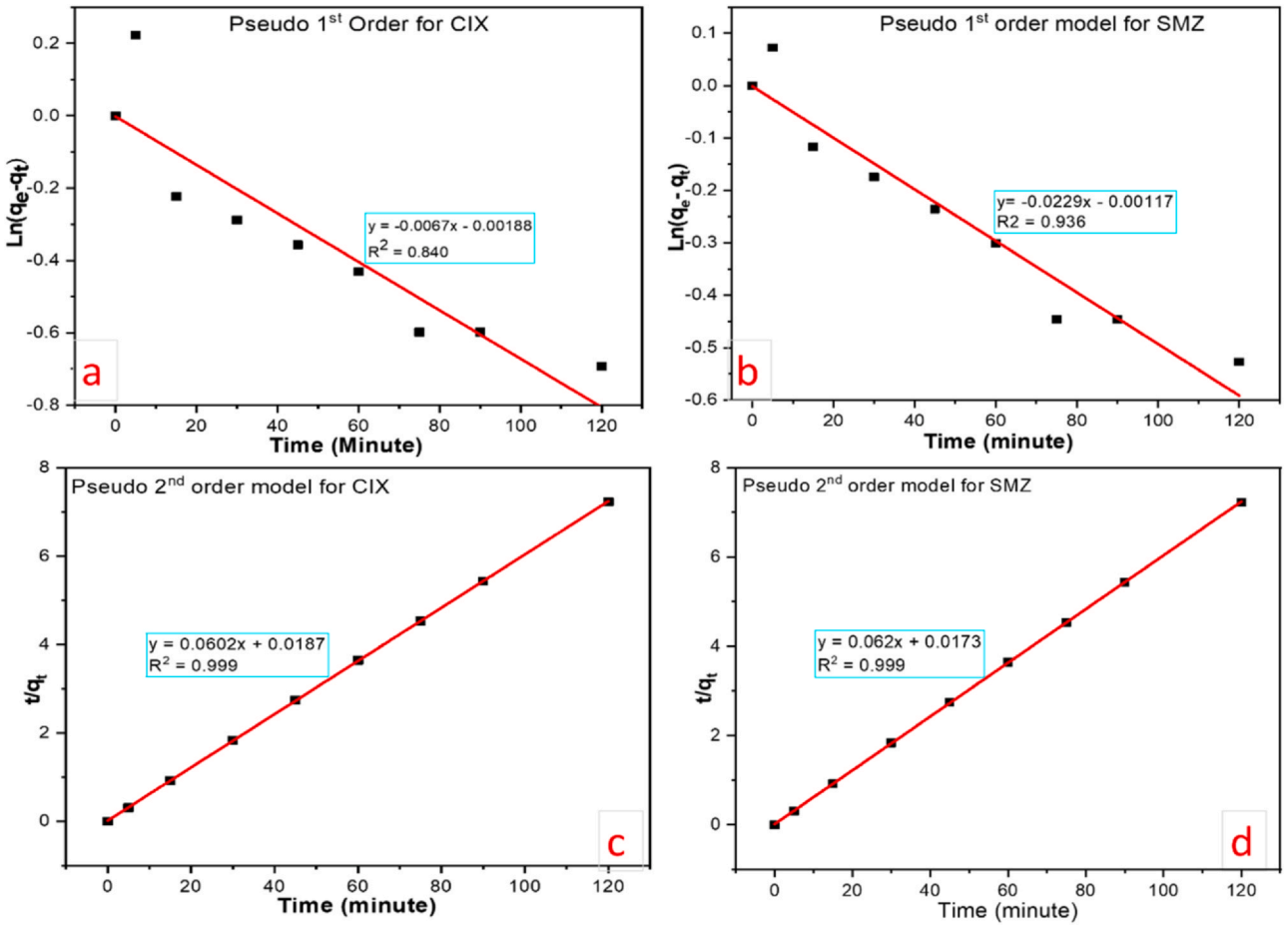

Fig. 13. Parameters of the kinetic model for the adsorption of CIX and SMZ, (a), Pseudo 1st order for CIX, (b) Pseudo 1st order for SMZ, (c) Pseudo 2nd order for CIX and (d) Pseudo 2nd order.

align with previous studies. While the average removal efficiency of both pollutants was around 98 % at 5 mg/L, it decreased to about 62 % and 65 % for CIX and SMZ respectively as the concentrations increased to 65 mg/L. This decrease may indicate the possibility of saturation of existing active sites of adsorbents and increasing the concentration of pollutants. This suggests that both adsorption capacity and removal efficiency improve with higher initial concentrations. These observations highlight the importance of thorough research on multi-component adsorption systems to enhance pollutant removal in complex environmental settings [72]. The detailed statements provide valuable insights for the optimal design and enhancement of adsorption-based wastewater treatment systems.

3.2.2. Effect of pH

The pH level of the solution significantly influences the adsorption of SMZ and CIX onto PJB. By adjusting the pH from 3 to 11, it was found that the removal efficiency of SMZ increased from pH 3 to 8. This is due to the biochar surface becoming increasingly negatively charged, which enhances the attraction of positively charged forms of CIX and SMZ at lower pH, and effectively adsorbs zwitterionic or neutral forms of CIX and negatively charged SMZ at higher pH. However, as pH increases above 8, the removal efficiency and q_e for both pollutants decrease due to increased electrostatic repulsion between the negatively charged biochar and the negatively charged forms of CIX and SMZ. .

The solubility of these compounds also varies with pH; in acidic conditions, they are more likely to be in less soluble protonated forms, while in basic conditions, their ionized forms are more soluble but less effectively adsorbed. At higher pH (basic conditions), they are more likely to be in their anionic forms, which tend to be more soluble. So, under varying pH conditions, the adsorption efficiency ranges from 79.2 to 98.7 % for SMZ and from 67.4 to 97.8 % for CIX. Regarding removal efficiency, SMZ demonstrates a wider range of pH compared to CIX. The study suggests that the behavior of SMZ and CIX molecules as anionic, cationic, and zwitterionic species at different pH levels accounts for these results [73]. The sorption process onto biochar sorbents may involve mechanisms such as hydrogen bonding and hydrophobic interfaces due to the occurrence of zwitterionic and anionic forms, indicating potential electron donor-acceptor interactions [74].

3.2.3. Adsorbent dose

The effect of different quantities of biochar on the adsorption of SMZ and CIX can be seen in Fig. 10. The findings showed that as the dose rose from 0.5 to 3 g/L, the amount of SMZ and CIX adsorbed per unit mass of biochar gradually fell from 2.8 to 0.05 mg/g. This reduction in adsorption capacity was due to the adsorbed ratio of SMZ and CIX ions to active sites as the mass of the adsorbent increased. However, the effectiveness of SMZ and CIX removal increased considerably from 74.5 to 98.6 % for SMZ and 71.8 to 98.4 % for CIX when the adsorbent dose increased from 0.5 to 1.5 g/L [75]. It then continued to increase steadily to 99.8 % at 3 g/L of biochar. This improvement in removal efficiency was attributed to the increase in active sites with a higher number of adsorbents. However, it should be noted that higher adsorbent doses could form a thicker adsorbent layer on the surface of the material. This could lead to diffusion limitations and slower pollutant removal rates. While higher adsorbent doses may initially enhance adsorption capacity, the thickening of the adsorbent layer could eventually yield diminishing returns and slower pollutant removal rates.

3.2.4. Impact of temperature and thermodynamics

The effect of temperature on the adsorption of SMZ and CIX was studied within the range of 25 to 50°C with the results depicted in Fig. 11*a* and *b*. Consistent with previous studies [76], the adsorption capacity increased with rising temperature. This phenomenon can be attributed to the heat supplied acting as activation energy, facilitating adsorption. Alternatively, the rise in adsorption with temperature suggests that the process may be governed by physisorption. This occurrence, referred to as temperature-enhanced adsorption, occurs when adsorbate molecules reveal a greater affinity for the adsorbent surface at higher temperatures. This can be attributed to changes in the thermodynamic driving forces governing the adsorption process, such as alterations in the enthalpy and entropy of adsorption. The removal efficiency of the adsorbent was increased with the temperature rise, showing an endothermic process. The temperature-dependent enhancement of adsorption capacity suggests that the adsorption mechanism may predominantly involve physisorption processes, where weak intermolecular forces play a significant role in adsorbate binding to the adsorbent surface ([77]. This insight provides a valuable understanding of the fundamental mechanisms governing the adsorption behavior of SMZ and CIX on PJ biochar. The endothermic nature of the adsorption process, evidenced by the increase in pollutant removal efficiency with rising temperature, suggests that heat is absorbed during the adsorption process [78]. This finding holds implications for the design and operation of adsorption-based wastewater treatment systems where controlling temperature can be utilized to optimize pollutant removal efficiency and energy consumption.

Similarly, the thermodynamic parameters value of ΔH was 8.950 J/mol, indicating an endothermic adsorption process. The calculated ΔG values at different temperatures (298.15 to 323.15 K) ranged from −0.092 to −0.850 J/mol, demonstrating that the adsorption of the studied compounds CIX and SMZ onto the adsorbent material was favorable and spontaneous under the given conditions. Moreover, the positive value of ΔS 0.0303 J/mol·K suggests an increase in randomness at the solid-liquid interface during adsorption. These indicate that the adsorption process of CIX and SMZ is not only energetically favorable but also driven by an increase in entropy, highlighting the potential applicability of the adsorbent material for the efficient removal of these pollutants from aqueous solutions. Further investigations could explore the kinetics and mechanisms underlying this adsorption process to enhance its practical utility in wastewater treatment applications.

3.3. Adsorption isotherms

Various isotherm models were used to study the adsorption of SMZ and CIX on the prepared PJ biochar which is indicated in Table 2, a comparison across references is presented in Table 3 and the graph is depicted in Fig. 12a-h. The adsorption isotherm shows how the adsorbed particles are distributed on the adsorbent. Linear and nonlinear regression models were used to determine the adsorption constants of the Langmuir, Freundlich, Temkin, and Dubinin-Radushkevich models. Both Langmuir and Freundlich isotherm models showed a strong fit for both pollutants, with an R^2 value close to 0.997. Langmuir isotherm explains that the adsorption process is a monolayer and limited adsorption [79], while Freundlich isotherm is an indicator of multilayer physical adsorption. The maximum adsorption capacity (q_{max}) was measured at 49.8 and 91.4 mg/g for SMZ and CIX, respectively. The binding energy constant (K_L) was found to be 0.036 for SMZ and 0.0187 for CIX. These results indicate a successful adsorption process, demonstrating the effectiveness of the interaction between the adsorbent and anionic SMZ and CIX in pharmaceutical wastewater. This suggests that the process may involve a monolayer adsorption mechanism [5].

3.4. Adsorption kinetics

To better understand how CIX and SMZ adsorbed on the adsorbent material, kinetic studies were carried out and the results are presented in Table 4. The high R^2 = 0.99 for both CIX and SMZ shows that the pseudo-second-order kinetic model produced a strong correlation, suggesting a probable rate-limiting step involving chemical adsorption processes, such as valence forces through electron-sharing [84]. The significant coherence between experimental and computed data further validates the application of the pseudo-second-order model in revealing the adsorption kinetics. In this study, the q_t value obtained of 16.606 mg/g estimated by the pseudo-second-order kinetic model is closer to the experimental q_e value of 16.689 mg/g found for the adsorption of CIX and SMZ onto PJ biochar [85]. However, the intra-particle diffusion model did not show a linear correlation that passes through the origin that is shown by the intra-particle diffusion plot. This disparity implies that the rate-limiting stage is not only governed by the intra-particle diffusion [86]. The lack of a linear plot suggests that many stages or other factors affect the total adsorption kinetics. In the first stage of IPD, residues are rapidly diffused through the solution to the bare exterior surface sorption sites on PJ biochar as a boundary layer diffusion step. The initial concentration provided the driving force to overcome mass transfer resistance between solid and liquid phases. The secondary stage was the IPD across macropores on the surface of PJ biochar and with the gradual sorption, the adsorption rate gradually slowed down because of the hindrance of intermolecular collision and inter-porous-channel extrusion, and the active sites on biochar were occupied increasingly. In the third stage, SMZ and CIX molecules moved through narrow pore channels to the micro-mesoporous of interior PJ biochar, the intraparticle diffusion rate was lower than in the former stage of surface diffusion. Finally, the adsorption rate was equivalent to the desorption rate, the surface adsorption tended to be balanced.

The well-fitted pseudo-second-order kinetics, along with the non-linear intra-particle diffusion graphs, suggest that chemical adsorption is the main factor influencing the overall kinetics. However, the adsorption process involves other significant factors. This may encompass external mass transfer resistance, which signifies the impact of boundary layer diffusion or film diffusion, particularly during the early phases of adsorption. The departure from the intra-particle diffusion model emphasizes the intricate character of the adsorption mechanism, wherein many processes may simultaneously contribute to the overall absorption of CIX and SMZ. This multimodal adsorption pattern has been found in similar investigations on pharmaceutical adsorption [87]. The combination of pseudo-second-order kinetics and non-linear intra-particle diffusion shows that the adsorption of CIX and SMZ includes a complicated interaction of chemical adsorption and mass transfer mechanisms. Understanding these complicated dynamics is vital for creating successful adsorption techniques for medication removal from aqueous solutions. .

3.5. Adsorption of real wastewater

Real pharmaceutical wastewater characterization was conducted, and the result obtained was compared with the literature and the detail is depicted in Table 5. The pH of real wastewater was slightly reduced from 6.78 to 6.70 post-treatment, agreeing with acceptable limits but falling short of the literature's proposed ideal pH of 7.2. If the initial pH is significantly greater than the pHpzc of the adsorbent, may act as a proton acceptor, leading to a decrease in pH [88]. Notably, total dissolved solid displayed a considerable decrease from 1109 to 151 mg/L, this may suggest the efficacy of biochar in eliminating dissolved particles. The conductivity increases from 2228 to 2567 μS/cm, while lower than the published value of 7253 μS/cm, this may be because pharmaceutical wastewater contains dissolved salts that are not effectively removed by the adsorption process. If the concentration of salts in the remaining water increases, it can contribute to higher conductivity [89]. Salinity climbed from 1.13 to 1.55, within permitted limits but indicating variations in ion concentrations, this may occur due to the adsorbent containing inorganic salt [90]. Turbidity observed a dramatic reduction from 450 NTU to 70 NTU, displaying effective clarity, this

shows that colloidal particles in the water, which contribute to turbidity, can be adsorbed onto the surface of the adsorbent material because of its high surface area [91]. The biochar displayed excellent performance in lowering TOC from 1050 to 124 mg/L. This may happen because the combination of various mechanisms, including adsorption, chemisorption, and surface reactivity, can synergistically contribute to the overall reduction in TOC [92,93]. BOD and COD were considerable declines from 762 to 98 mg/L and 2498 to 541 mg/L, respectively. This may happen because the combined effects of microbial activity, adsorption, and surface reactivity contribute synergistically to the effective decomposition of organic matter, resulting in significant declines in both BOD and COD [94]. However, the decrease in nitrate concentrations from 57 to 12.1 mg/L and sulfate concentrations from 82 to 47 mg/L, when nitrate and sulfate were initially part of more complex organic or inorganic compounds, the adsorption process may involve the breakdown or transformation of these parent compounds, leading to reduced nitrate and sulfate concentrations [95]. The concentrations of the target pollutants in the wastewater were determined to be 8.29 mg/L for CIX and 5.3 mg/L for SMZ. After treatment, the removal efficiency was 76.7 % for CIX and 80.4 % for SMZ. In conclusion, biochar demonstrates great potential for pharmaceutical industry wastewater treatment, however, fine-tuning is required to optimize certain parameters and assure compliance with optimal water quality requirements.

4. Conclusions

The plant PJ, widely known as a distributed weed, was utilized as a precursor material to synthesize low-cost, eco-friendly biochar. This biochar was used as a good adsorbent for SMZ and CIX removal from pharmaceutical industry wastewater. The characterization of the biochar was conducted to assess its surface properties and interaction with SMZ and CIX, employing techniques such as SEM, EDX, FTIR, BET, XRD, and TGA. The maximum removal efficiency of SMZ and CIX was 98.7 % and 97.8 % respectively at the optimum working conditions identified for each pollutant. The real wastewater was characterized in terms of COD and TOC and the biochar treatment was reducing the pollutants from 2498 to 514 mg/L and 1050 to 124 mg/L, respectively. Target pollutants concentration in real wastewater was found to be 8.29 and 5.3 mg/L for CIX and SMZ and their removal efficiency was obtained as 80.4 % and 76.7 %, respectively. Among the isotherm models tested, Langmuir was found to best fit experimental data with an R^2 0.99, indicating a homogeneous and monolayer adsorption surface. The experimental data also confirmed outstanding agreement with pseudo-second-order kinetics (R^2 ~0.99) for both pollutants. However, the non-linear intra-particle diffusion graphs suggested that chemical adsorption plays a substantial role in the overall kinetics. Therefore, the biochar-based adsorbent presents itself as a viable, low-cost, locally available solution for treating industrial wastewater, with the potential for scaling up to an industrial level as a sustainable material for environmental remediation.

Ethical approval

Not applicable.

Funding

This research was funded by Addis Ababa Science and Technology University (AASTU).

CRediT authorship contribution statement

Abebe Worku: Writing – review & editing, Writing – original draft, Resources, Project administration, Formal analysis. **Jemal Fito:** Writing – review & editing, Writing – original draft, Visualization, Validation, Supervision, Software, Project administration, Methodology, Funding acquisition, Formal analysis, Data curation, Conceptualization. **Titus A.M. Msagati:** Writing – review & editing, Writing – original draft. **Hailu Ashebir:** Writing – review & editing, Writing – original draft, Software, Methodology, Investigation, Formal analysis, Conceptualization.

Data Availability

Data will be made available on request.

Declaration of Competing Interest

The authors declare that they have no known competing financial interests or personal relationships that could have appeared to influence the work reported in this paper.

Acknowledgment

The authors would like to thank Addis Ababa Science and Technology University, Department of Environmental Engineering for financial support and laboratory services.

Authors contributions

All authors have contributed to this paper, the concept development HA and JN, draft preparation and revision by HA, AW, JN, and TM, and approved submission HA, AW, JN, and TM.

Consent to participate

Not applicable.

Consent to publish

Not applicable.

References

[1] Martinho SD, Fernandes VC, Figueiredo SA, Delerue-Matos C. Microplastic pollution focused on sources, distribution, contaminant interactions, analytical methods, and wastewater removal strategies: a review. Int J Environ Res Public Health 2022;19:5610.
[2] Thiebault T. Sulfamethoxazole/Trimethoprim ratio as a new marker in raw wastewaters: a critical review. Sci Total Environ 2020;715:136916.
[3] Cincinelli A, Martellini T, Coppini E, Fibbi D, Katsoyiannis A. Nanotechnologies for removal of pharmaceuticals and personal care products from water and wastewater. a review. J Nanosci Nanotechnol 2015;15:3333–47. https://doi.org/10.1166/jnn.2015.10036.
[4] Chiș AA, Rus LL, Morgovan C, Arseniu AM, Frum A, Vonica-Țincu AL, et al. Microbial resistance to antibiotics and effective antibiotherapy. Biomedicines 2022;10:1121.
[5] Subramaniyasharma S, Shanmugam SR, Bhuvaneswari V, Ponnusami V, Rangabhashiyam S. Pyrolysis of an invasive weed Prosopis juliflora wood biomass for the adsorptive removal of ciprofloxacin. Biomass– Convers Biorefin. 2023:1–16.
[6] Tuitert G.B. Assessing and quantifying the pharmaceutical supply chain and its environmental impacts 2021.
[7] Anh HQ, Le TPQ, Da Le N, Lu XX, Duong TT, Garnier J, et al. Antibiotics in surface water of East and Southeast Asian countries: a focused review on contamination status, pollution sources, potential risks, and future perspectives. Sci Total Environ 2021;764:142865.
[8] Pradhan B, Chand S, Chand S, Rout PR, Naik SK. Emerging groundwater contaminants: a comprehensive review on their health hazards and remediation technologies. Ground Sustain Dev 2023;20:100868.
[9] Nguyen M-K, Lin C, Nguyen H-L, Hung NTQ, La DD, Nguyen XH, et al. Occurrence, fate, and potential risk of pharmaceutical pollutants in agriculture: challenges and environmentally friendly solutions. Sci Total Environ 2023;899:165323.
[10] Nas B, Dolu T, Koyuncu S. Behavior and removal of ciprofloxacin and sulfamethoxazole antibiotics in three different types of full-scale wastewater treatment plants: a comparative study. Water, Air, Soil Pollut 2021;232:127.

[11] Langbehn RK, Michels C, Soares HM. Antibiotics in wastewater: From its occurrence to the biological removal by environmentally conscious technologies. Environ Pollut 2021;275:116603.
[12] Kim D-W, Cha C-J. Antibiotic resistome from the One-Health perspective: understanding and controlling antimicrobial resistance transmission. Exp Mol Med 2021;53:301–9.
[13] Larsson DGJ, Flach C-F. Antibiotic resistance in the environment. Nat Rev Microbiol 2022;20:257–69.
[14] Amábile-Cuevas CF. Antibiotics and antibiotic resistance in the environment. CRC Press; 2015.
[15] Phoon BL, Ong CC, Mohamed Saheed MS, Show PL, Chang JS, Ling TC, et al. Conventional and emerging technologies for removal of antibiotics from wastewater. J Hazard Mater 2020;400:122961. https://doi.org/10.1016/j.jhazmat.2020.122961.
[16] Krzeminski P, Tomei MC, Karaolia P, Langenhoff A, Almeida CMR, Felis E, et al. Performance of secondary wastewater treatment methods for the removal of contaminants of emerging concern implicated in crop uptake and antibiotic resistance spread: a review. Sci Total Environ 2019;648:1052–81. https://doi.org/10.1016/j.scitotenv.2018.08.130.
[17] Fu J, Zhao Y, Yao Q, Addo-Bankas O, Ji B, Yuan Y, et al. A review on antibiotics removal: Leveraging the combination of grey and green techniques. Sci Total Environ 2022;838:156427.
[18] Wang J, Wang S. Reactive species in advanced oxidation processes: formation, identification and reaction mechanism. Chem Eng J 2020;401:126158.
[19] Karimi-Maleh H, Darabi R, Karimi F, Karaman C, Shahidi SA, Zare N, et al. State-of-art advances on removal, degradation and electrochemical monitoring of 4-aminophenol pollutants in real samples: a review. Environ Res 2023:115338.
[20] Umar M, Aziz HA. Photocatalytic degradation of organic pollutants in water. Org Pollut Risk Treat 2013;8:196–7.
[21] Ahmed SF, Mofijur M, Nuzhat S, Chowdhury AT, Rafa N, Uddin MA, et al. Recent developments in physical, biological, chemical, and hybrid treatment techniques for removing emerging contaminants from wastewater. J Hazard Mater 2021;416:125912. https://doi.org/10.1016/j.jhazmat.2021.125912.
[22] Fito J, Nkambule TTI. Synthesis of biochar-CoFe2O4 nanocomposite for adsorption of methylparaben from wastewater under full factorial experimental design. Environ Monit Assess 2023;195. https://doi.org/10.1007/s10661-022-10819-w.
[23] Abewaa M, Mengistu A, Takele T, Fito J, Nkambule T. Adsorptive removal of malachite green dye from aqueous solution using Rumex abyssinicus derived activated carbon. Sci Rep 2023;13:14701. https://doi.org/10.1038/s41598-023-41957-x.
[24] Rashid R, Shafiq I, Akhter P, Iqbal MJ, Hussain M. A state-of-the-art review on wastewater treatment techniques: the effectiveness of adsorption method. Environ Sci Pollut Res 2021;28:9050–66. https://doi.org/10.1007/s11356-021-12395-x.
[25] Priyadarshini M, Das I, Ghangrekar MM, Blaney L. Advanced oxidation processes: performance, advantages, and scale-up of emerging technologies. J Environ Manag 2022;316:115295.
[26] Zhang S, Zheng H, Tratnyek PG. Advanced redox processes for sustainable water treatment. Nat Water 2023;1:666–81.
[27] Sabzehmeidani MM, Mahnaee S, Ghaedi M, Heidari H, Roy VAL. Carbon based materials: a review of adsorbents for inorganic and organic compounds. Mater Adv 2021;2:598–627.
[28] Scaria J, Gopinath A, Ranjith N, Ravindran V, Ummar S, Nidheesh PV, et al. Carbonaceous materials as effective adsorbents and catalysts for the removal of emerging contaminants from water. J Clean Prod 2022;350:131319.
[29] Kwak CH, Lim C, Kim S, Lee Y-S. Surface modification of carbon materials and its application as adsorbents. J Ind Eng Chem 2022.
[30] Rathi BS, Kumar PS. Application of adsorption process for effective removal of emerging contaminants from water and wastewater. Environ Pollut 2021;280:116995. https://doi.org/10.1016/j.envpol.2021.116995.
[31] Fito J, Kefeni KK, Nkambule TTI. The potential of biochar-photocatalytic nanocomposites for removal of organic micropollutants from wastewater. Sci Total Environ 2022;829:154648. https://doi.org/10.1016/j.scitotenv.2022.154648.
[32] Prasannamedha G, Kumar PS, Mehala R, Sharumitha TJ, Surendhar D. Enhanced adsorptive removal of sulfamethoxazole from water using biochar derived from hydrothermal carbonization of sugarcane bagasse. J Hazard Mater 2021;407:124825.
[33] He M, Xu Z, Hou D, Gao B, Cao X, Ok YS, et al. Waste-derived biochar for water pollution control and sustainable development. Nat Rev Earth Environ 2022;3:444–60.
[34] Chandra S, Jagdale P, Medha I, Tiwari AK, Bartoli M, Nino A, et al. Biochar-supported TiO2-based nanocomposites for the photocatalytic degradation of sulfamethoxazole in water—A review. Toxics 2021;9:313.
[35] Zungu V, Hadebe L, Mpungose P, Hamza I, Amaku J, Gumbi B. Fabrication of biochar materials from biowaste coffee grounds and assessment of its adsorbent efficiency for remediation of water-soluble pharmaceuticals. Sustainability 2022;14:2931.
[36] Świechowski K, Rasaq WA, Stegenta-Dąbrowska S, Białowiec A. Characterization of Engineered Biochar: Proximate Analyses, Ultimate Analyses, Physicochemical Analyses, Surface Analyses, and Molecular Analyses. Eng. Biochar Fundam. Prep. Charact. Appl. Springer,; 2022. p. 127–48.
[37] Seow YX, Tan YH, Mubarak NM, Kansedo J, Khalid M, Ibrahim ML, et al. A review on biochar production from different biomass wastes by recent carbonization technologies and its sustainable applications. J Environ Chem Eng 2022;10:107017.
[38] Jagadeesh N, Sundaram B. Adsorption of pollutants from wastewater by biochar: a review. J Hazard Mater Adv 2023;9:100226.
[39] Kazemi Shariat Panahi H, Dehhaghi M, Ok YS, Nizami AS, Khoshnevisan B, Mussatto SI, et al. A comprehensive review of engineered biochar: production, characteristics, and environmental applications. J Clean Prod 2020;270:122462. https://doi.org/10.1016/j.jclepro.2020.122462.
[40] Fito J, Tibebu S, Nkambule TTI. Optimization of Cr (VI) removal from aqueous solution with activated carbon derived from Eichhornia crassipes under response surface methodology. BMC Chem 2023;17:1–19. https://doi.org/10.1186/s13065-023-00913-6.
[41] Gupta SV, Kulkarni VV, Ahmaruzzaman M. Fabrication of a bio-adsorbent material by grafting CeO2 quantum dots (QDts) over Areca nut shell biochar using Saccharum officinarum extract as a solvent/capping agent for adsorption of Methylene blue dye: Synthesis, material analyses, adsorption kinetic. Colloids Surf A Physicochem Eng Asp 2024;680:132611.
[42] Orimolade BO, Arotiba OA. Towards visible light driven photoelectrocatalysis for water treatment: application of a FTO/BiVO4/Ag2S heterojunction anode for the removal of emerging pharmaceutical pollutants. Sci Rep 2020;10:5348.
[43] Scott E. Remediation of ciprofloxacin hydrochloride-contaminated wastewater by Phragmites australis biosorbent 2020.
[44] Laskar II, Hashisho Z. Insights into modeling adsorption equilibria of single and multicomponent systems of organic and water vapors. Sep Purif Technol 2020;241:116681.
[45] Araújo CST, Almeida ILS, Rezende HC, Marcionilio SMLO, Léon JJL, de Matos TN. Elucidation of mechanism involved in adsorption of Pb (II) onto lobeira fruit (Solanum lycocarpum) using Langmuir, Freundlich and Temkin isotherms. Microchem J 2018;137:348–54.
[46] Baky MAH, Rahman MM, Islam AKMS. Development of renewable energy sector in Bangladesh: Current status and future potentials. Renew Sustain Energy Rev 2017;73:1184–97.
[47] Tong S, Zhang S, Yin H, Wang J, Chen M. Study on co-hydrothermal treatment combined with pyrolysis of rice straw/sewage sludge: biochar properties and heavy metals behavior. J Anal Appl Pyrolysis 2021;155:105074.
[48] Kumar R, Chandrashekar N. Study on fuelwood and carbonization characteristics of Prosopis juliflora. J Indian Acad Wood Sci 2016;13:101–7.
[49] Cantrell KB, Hunt PG, Uchimiya M, Novak JM, Ro KS. Impact of pyrolysis temperature and manure source on physicochemical characteristics of biochar. Bioresour Technol 2012;107:419–28.
[50] Lehmann J, Joseph S. Biochar for environmental management: science, technology and implementation. Routledge,; 2015.
[51] Ahmad M, Rajapaksha AU, Lim JE, Zhang M, Bolan N, Mohan D, et al. Biochar as a sorbent for contaminant management in soil and water: a review. Chemosphere 2014;99:19–33. https://doi.org/10.1016/j.chemosphere.2013.10.071.
[52] Sutradhar M, Barman TR, Mukherjee G, Kar M, Saha SS, Drew MGB, et al. Malonato complexes of oxidovanadium(IV): Synthesis, structural characterization and exploration of their insulin mimetic properties. Inorg Chim Acta 2011;368:13–20. https://doi.org/10.1016/j.ica.2010.12.018.
[53] Gayathri G, Uppuluri KB. The comprehensive characterization of Prosopis juliflora pods as a potential bioenergy feedstock. Sci Rep 2022;12:18586.
[54] Patidar R, Srivastava VC. Mechanistic and kinetic insights of synergistic mineralization of ofloxacin using a sono-photo hybrid process. Chem Eng J 2021;403:125736.
[55] Karim AV, Shriwastav A. Degradation of ciprofloxacin using photo, sono, and sonophotocatalytic oxidation with visible light and low-frequency ultrasound: degradation kinetics and pathways. Chem Eng J 2020;392:124853. https://doi.org/10.1016/J.CEJ.2020.124853.
[56] Gale M, Nguyen T, Moreno M, Gilliard-AbdulAziz KL. Physiochemical properties of biochar and activated carbon from biomass residue: influence of process conditions to adsorbent properties. ACS Omega 2021;6:10224–33.
[57] Stankeviča K. Character of sapropel properties based on its formation conditionsand possibilities of its use 2020.
[58] Pesonen J., Sauvola E., Hu T., Tuomikoski S. Use of side stream-based $MgSO_4$ as chemical precipitant in the simultaneous removal of nitrogen and phosphorus from wastewaters 2020.
[59] Saravanakumar SS, Kumaravel A, Nagarajan T, Sudhakar P, Baskaran R. Characterization of a novel natural cellulosic fiber from Prosopis juliflora bark. Carbohydr Polym 2013;92:1928–33.
[60] Ural N. The significance of scanning electron microscopy (SEM) analysis on the microstructure of improved clay: An overview. Open Geosci 2021;13:197–218.
[61] Kumar S, Saha A. Utilization of coconut shell biomass residue to develop sustainable biocomposites and characterize the physical, mechanical, thermal, and water absorption properties. Biomass– Convers Biorefin 2022:1–17.
[62] Bhat S, Uthappa UT, Sadhasivam T, Altalhi T, Han SS, Kurkuri MD. Abundant cilantro derived high surface area activated carbon (AC) for superior adsorption performances of cationic/anionic dyes and supercapacitor application. Chem Eng J 2023;459:141577.
[63] Ma X, Deng J, Zhang R, Li S, Zhang R. Hierarchical porous carbon nanoarchitectonics with honeycomb-like and N, P co-doped features for flexible symmetric supercapacitors and high-efficiency dye removal. J Energy Storage 2023;65:107272. https://doi.org/10.1016/j.est.2023.107272.
[64] Zhao Y, Min X, Huang Z, Liu Y, Wu X, Fang M. Honeycomb-like structured biological porous carbon encapsulating PEG: A shape-stable phase change material with enhanced thermal conductivity for thermal energy storage. Energy Build 2018;158:1049–62. https://doi.org/10.1016/j.enbuild.2017.10.078.
[65] Fito J, Mengistu A, Abewaa M, Angassa K, Moyo W, Phiri Z, et al. Adsorption of Black MNN reactive dye from tannery wastewater using activated carbon of Rumex Abysinicus. J Taiwan Inst Chem Eng 2023;151:105138. https://doi.org/10.1016/j.jtice.2023.105138.
[66] Mourdikoudis S, Pallares RM, Thanh NTK. Characterization techniques for nanoparticles: comparison and complementarity upon studying nanoparticle properties. Nanoscale 2018;10:12871–934.

[67] Jeyaraj M, Gurunathan S, Qasim M, Kang M-H, Kim J-H. A comprehensive review on the synthesis, characterization, and biomedical application of platinum nanoparticles. Nanomaterials 2019;9:1719.
[68] McClelland JF, Jones RW, Luo S, Seaverson LM. A practical guide to FT-IR photoacoustic spectroscopy. Pract. Sampl. Tech. infrared Anal. CRC Press; 2020. p. 107–44.
[69] Chen Y, Zou C, Mastalerz M, Hu S, Gasaway C, Tao X. Applications of micro-fourier transform infrared spectroscopy (FTIR) in the geological sciences—a review. Int J Mol Sci 2015;16:30223–50.
[70] Rajan BS, Balaji MAS, Saravanakumar SS. Effect of chemical treatment and fiber loading on physico-mechanical properties of Prosopis juliflora fiber reinforced hybrid friction composite. Mater Res Express 2018;6:35302.
[71] Böke JS, Popp J, Krafft C. Optical photothermal infrared spectroscopy with simultaneously acquired Raman spectroscopy for two-dimensional microplastic identification. Sci Rep 2022;12:18785.
[72] Ghosh S, Pourebrahimi S, Malloum A, Ajala OJ, AlKafaas SS, Onyeaka H, et al. A review on ciprofloxacin removal from wastewater as a pharmaceutical contaminant: covering adsorption to advanced oxidation processes to computational studies. Mater Today Commun 2023:107500.
[73] Zhang L, Shen S. Adsorption and catalytic degradation of sulfamethazine by mesoporous carbon loaded nano zero valent iron. J Ind Eng Chem 2020;83:123–35.
[74] Maged A, Elgarahy AM, Hlawitschka MW, Haneklaus NH, Gupta AK, Bhatnagar A. Synergistic mechanisms for the superior sorptive removal of aquatic pollutants via functionalized biochar-clay composite. Bioresour Technol 2023;387:129593.
[75] Li Y, Zhu Y, Yan X, Zhang G, Yan G, Li H. Strategy and mechanisms of sulfamethoxazole removal from aqueous systems by single and combined Shewanella oneidensis MR-1 and nanoscale zero-valent iron-enriched biochar. Sci Total Environ 2023;883:163676.
[76] Luo B, Huang G, Yao Y, An C, Zhang P, Zhao K. Investigation into the influencing factors and adsorption characteristics in the removal of sulfonamide antibiotics by carbonaceous materials. J Clean Prod 2021;319:128692.
[77] Al-Ghouti MA, Al-Absi RS. Mechanistic understanding of the adsorption and thermodynamic aspects of cationic methylene blue dye onto cellulosic olive stones biomass from wastewater. Sci Rep 2020;10:15928.
[78] Allahkarami E, Dehghan Monfared A, Silva LFO, Dotto GL. Toward a mechanistic understanding of adsorption behavior of phenol onto a novel activated carbon composite. Sci Rep 2023;13:167.
[79] Koklu R, Imamoglu M. Removal of ciprofloxacin from aqueous solution by activated carbon prepared from orange peel using zinc chloride. Membr Water Treat 2022;13:129–37.
[80] Yang Z, Xing R, Zhou W, Zhu L. Adsorption characteristics of ciprofloxacin onto g-MoS 2 coated biochar nanocomposites. Front Environ Sci Eng 2020;14:1–10.
[81] Afzal MZ, Sun X-F, Liu J, Song C, Wang S-G, Javed A. Enhancement of ciprofloxacin sorption on chitosan/biochar hydrogel beads. Sci Total Environ 2018;639:560–9.
[82] Shearer L, Pap S, Gibb SW. Removal of pharmaceuticals from wastewater: a review of adsorptive approaches, modelling and mechanisms for metformin and macrolides. J Environ Chem Eng 2022;10:108106.
[83] Zubair M, Saliq Q, Manzar MS, Aziz HA, Haroon H, Hung Y-T, et al. Biochar for adsorptive removal of pharmaceuticals from environmental water. Waste Treat. Biotechnol. Agric. Food Ind Vol. 2. Springer; 2023. p. 199–225.
[84] Revellame ED, Fortela DL, Sharp W, Hernandez R, Zappi ME. Adsorption kinetic modeling using pseudo-first order and pseudo-second order rate laws: a review. Clean Eng Technol 2020;1:100032.
[85] Özer Ç, İmamoğlu M. Isolation of nickel (II) and lead (II) from aqueous solution by sulfuric acid prepared pumpkin peel biochar. Anal Lett 2023;56:491–503.
[86] Di Plinio S. Testing the magnitude of correlations across experimental conditions. Front Psychol 2022;13:860213.
[87] Wang J, Guo X. Rethinking of the intraparticle diffusion adsorption kinetics model: Interpretation, solving methods and applications. Chemosphere 2022;309:136732.
[88] Shen L, Lu B, Li Y, Liu J, Huang-fu Z, Peng H, et al. Interfacial structure of water as a new descriptor of the hydrogen evolution reaction. Angew Chem Int Ed 2020;59:22397–402.
[89] Alam R, Khan SU, Usman M, Asif M, Farooqi IH. A critical review on treatment of saline wastewater with emphasis on electrochemical based approaches. Process Saf Environ Prot 2022;158:625–43.
[90] White CM, Smith DH, Jones KL, Goodman AL, Jikich SA, LaCount RB, et al. Sequestration of carbon dioxide in coal with enhanced coalbed methane recovery a review. Energy Fuels 2005;19:659–724.
[91] Febbraio T. The efficacy of two biochar variants as filtration material for the improvement of river water quality 2020.
[92] Tünay S., Köklü R., Imamoğlu M. Removal of diclofenac, ciprofloxacin and sulfamethoxazole from wastewater using granular activated carbon from hazelnut shell: isotherm, kinetic and thermodynamic studies. 2022.
[93] Zango ZU, Garba A, Garba ZN, Zango MU, Usman F, Lim J-W. Montmorillonite for adsorption and catalytic elimination of pollutants from Wastewater: a State-of-the-Arts review. Sustainability 2022;14:16441.
[94] Chan SS, Khoo KS, Chew KW, Ling TC, Show PL. Recent advances biodegradation and biosorption of organic compounds from wastewater: microalgae-bacteria consortium-A review. Bioresour Technol 2022;344:126159.
[95] Dia A, Gruau G, Olivié-Lauquet G, Riou C, Molénat J, Curmi P. The distribution of rare earth elements in groundwaters: assessing the role of source-rock composition, redox changes and colloidal particles. Geochim Cosmochim Acta 2000;64:4131–51.
[96] Ahmadi M, Ramezani Motlagh H, Jaafarzadeh N, Mostoufi A, Saeedi R, Barzegar G, et al. Enhanced photocatalytic degradation of tetracycline and real pharmaceutical wastewater using MWCNT/TiO2 nano-composite. J Environ Manag 2017;186:55–63. https://doi.org/10.1016/J.JENVMAN.2016.09.088.
[97] Pal A, Gin KY-H, Lin AY-C, Reinhard M. Impacts of emerging organic contaminants on freshwater resources: review of recent occurrences, sources, fate and effects. Sci Total Environ 2010;408:6062–9.
[98] Wajahat R, Yasar A, Khan AM, Tabinda AB, Bhatti SG. Ozonation and photo-driven oxidation of ciprofloxacin in pharmaceutical wastewater: degradation kinetics and energy requirements. Pol J Environ Stud 2019;28:1933.